ECOSYSTEMS

Inundation, Hydrodynamics and Vegetation Influence Carbon Dioxide Concentrations in Amazon Floodplain Lakes

João Henrique Fernandes Amaral,[1,2]* John Michael Melack,[1,3] Pedro Maia Barbosa,[1,4] Alberto V. Borges,[5] Daniele Kasper,[4] Alicia Cortes Cortés,[6] Wencai Zhou,[1] Sally MacIntyre,[1] and Bruce Rider Forsberg[2,7]

[1]Earth Research Institute, 6832 Ellison Hall, University of California, Santa Barbara, California, USA; [2]Coordenação de Dinâmica Ambiental, Laboratório de Ecossistemas Aquáticos, Instituto Nacional de Pesquisas da Amazônia, Manaus, Amazonas, Brazil; [3]Bren School of Environmental Science and Management, University of California, Santa Barbara, California, USA; [4]Centro de Ciências da Saúde, Universidade Federal Do Rio de Janeiro, Rio de Janeiro, Rio de Janeiro, Brazil; [5]Chemical Oceanography Unit, University of Liège, Liège, Belgium; [6]Marine Science Institute, University of California, Santa Barbara, California, USA; [7]Vermont Department of Environmental Conservation, Montpelier, Vermont, USA

ABSTRACT

Extensive floodplains and numerous lakes in the Amazon basin are well suited to examine the role of floodable lands within the context of the sources and processing of carbon within inland waters. We measured diel, seasonal and inter-annual variations of CO_2 concentrations and related environmental variables in open water and flooded vegetation and estimated their habitat area using remote sensing in a representative Amazon floodplain lake, Lake Janauacá. Variability in CO_2 concentrations in open water resulted from changes in the extent of inundation and exchange with vegetated habitats. Depth-averaged values of CO_2 in the open water of the lake, 157 ± 91 μM (mean $\pm$ SD), were less than those in an embayment near aquatic vegetation, 285 ± 116 μM, and were variable over 24-h periods at both sites. Within floating herbaceous plant mats, the mean concentration was 275 ± 77 μM, while in flooded forests it was 217 ± 78 μM. The best statistical model that included CO_2 in aquatic plant mats, water clarity, rate of change in water level and chlorophyll-*a* concentrations explained around 90% of the variability in CO_2 concentration. Three-dimensional hydrodynamic modeling demonstrated that diel differences in water temperature between plant mats and open water as well as basin-scale motions caused lateral exchanges of CO_2 between vegetated habitats and open water. Our findings extend understanding of CO_2 in tropical lakes and floodplains with measurements and models that emphasize the importance of flooded forests and aquatic herbaceous plants fringing floodplain lakes as sources of CO_2 to open waters.

HIGHLIGHTS

- Aquatic plants are major sources of CO_2 to open waters of floodplain lakes.
- Extended low water period enhanced CO_2 concentrations as inundated plants decayed.
- Diel changes in thermal gradients drive lateral exchange of CO_2.

INTRODUCTION

Carbon cycling in lakes integrates inputs from the landscape and biogeochemical and ecological processes within lakes (Tranvik and others 2009; Premke and others 2016; Kayler and others 2019). As a component of the active pipe hypothesis, lakes contribute to the processing, storing and emissions of carbon en route to oceans (Cole and others 2007). Carbon inputs from vegetated areas within the aquatic ecosystems can alter regional carbon balances (Amaral and others 2020; Drake and others 2018). Floodplain lakes, abundant in tropical and northern regions, receive organic and inorganic carbon from their catchments and from areas with submerged, floating and emergent plants.

Among river systems, the Amazon basin, with extensive floodplains and numerous lakes (Sippel and others 1992; Hess and others 2015), provides an ideal system to examine the role of floodable lands within the context of the active pipe hypothesis. Large seasonal and inter-annual variations in depth and extent of inundation create a seasonally flooded region called the aquatic-terrestrial transition zone (Junk and others 1989). As water levels rise, coverage of emergent and floating herbaceous plants expands and contracts (Junk and Piedade 1993; Engle and others 2008), fringing forests are inundated (Junk and others 2010), and open water areas expand. For example, an organic carbon balance for an Amazon floodplain lake by Melack and Engle (2009) found that annual inputs from the Solimões River and local runoff provided 94% of the water but only 8% of the organic carbon, while seasonal growth of floating herbaceous plants and litterfall from inundated forests contributed 72% of the organic carbon in the system.

Others have inferred the influence of aquatic vegetation on CO_2 concentrations based on higher concentrations near vegetated lake margins (Rudorff and others 2011) and in lakes with a larger percentage of vegetated floodplain (Abril and others 2014). Abril and Borges (2019) suggest that riparian and littoral wetlands have strong hydrological connectivity to inland waters and often are productive, assimilating atmospheric CO_2 and transferring a portion of the fixed carbon to the water.

As is common in lakes throughout the world (Sobek and others 2005; Marotta and others 2009; McDonald and others 2013), Amazon lakes are often supersaturated in carbon dioxide with respect to atmospheric equilibrium, though considerable spatial and temporal variations occur. For example, Rudorff and others (2011) reported a range from 47 to 233 µM at low water to maximum of 656 µM at high water in Lago Curuai, and Abril and others (2014) measured a range from 0.5 to 500 µM on transects in five lakes. Amaral and others (2019) sampled seven floodplain lakes along the Solimões River during four hydrological phases and reported near-surface concentrations among all the lakes to vary from 9.4 to 231 µM. All these data are from near-surface, open water habitats during daytime, and not from vegetated habitats or over diel periods. The variations in dissolved CO_2 are likely associated with biological and physical factors. Including aquatic and algal primary production (Engle and others 2008; Forsberg and others 2017a) and respiration (Amaral and others 2018), dissolved organic carbon (DOC) and its susceptibility to degradation (Ward and others 2013), inundation extent (Abril and others 2014) and watershed inputs (Johnson and others 2008). Variations in meteorological conditions, thermal stratification and mixing, exchange with the atmosphere, and lateral advection (MacIntyre and others 2019) can also contribute to variability in CO_2 concentrations.

To examine temporal and spatial variations in dissolved CO_2 in Amazon floodplain lakes and the physical and biological processes likely to influence these variations, we measured diel, seasonal and inter-annual variations of dissolved CO_2 and related environmental variables combined with remote sensing of flooded vegetation in a representative central Amazon floodplain lake, Lake Janauacá. The Janauacá floodplain has a large open water area close to the Solimões River and numerous embayments in close proximity to vegetated habitats. As is typical of central Amazon floodplains, the open waters are surrounded by
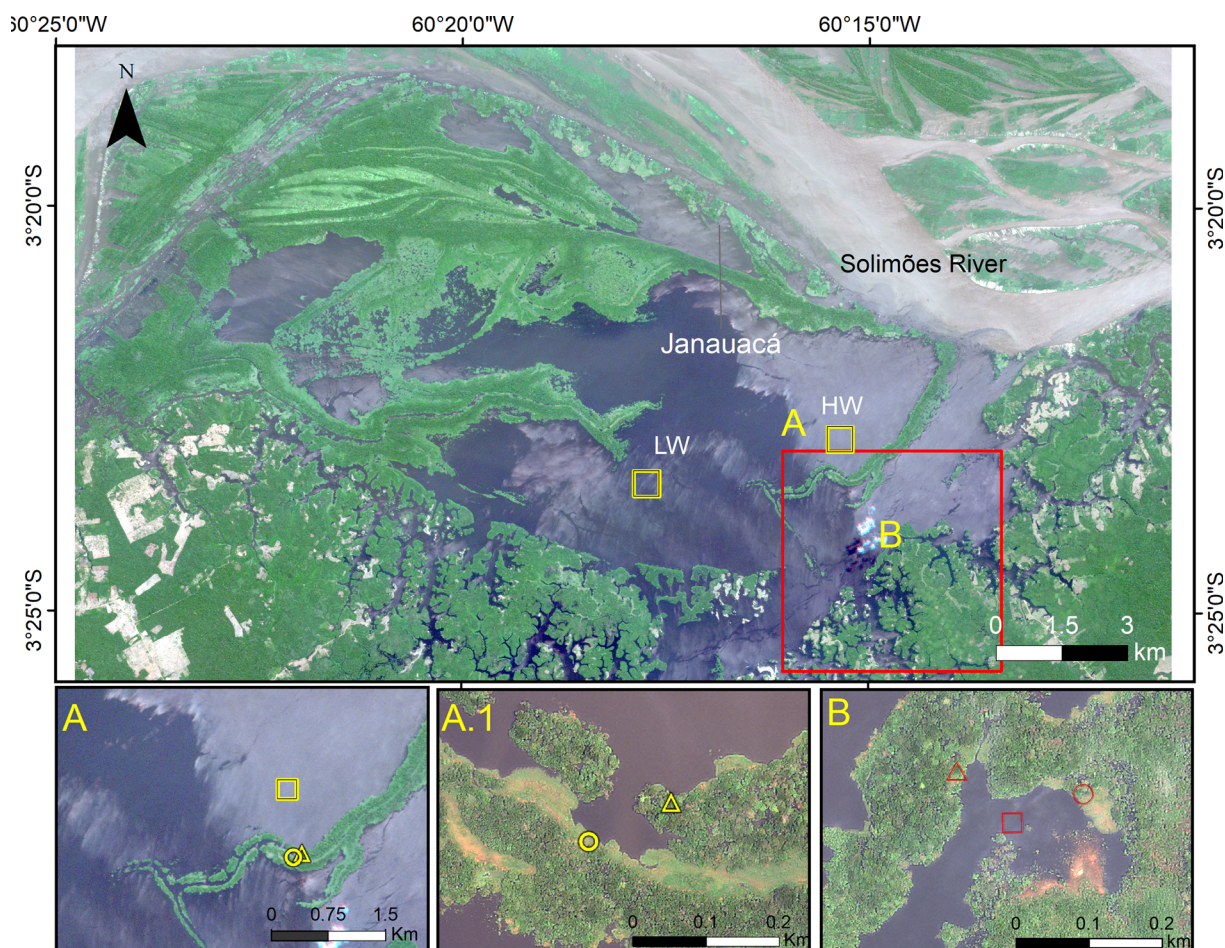
Figure 1. Lake Janauacá on the Solimões River floodplain. Upper panel **A** approximate locations of open lake sampling sites (OL) during high water (HW) and low water (LW). **B** embayment site (EM) and reference quadrant (25 km^2), used for estimation of areal coverage of herbaceous aquatic plants. Lower images are detailed views of habitats **A** and **A.1** (OL site): open water at HW (yellow square), flooded forest (yellow triangle) and floating plants (yellow circle). **B** (EM site): open water (red square), flooded forest (red triangle) and floating plants (red circle). Multispectral images: Upper and **A** Planet Scope Rapid-eye image acquired on 08/15/2015; **A.1** and **B** Apollo World View -2 image on 08/14/2014.

aquatic-terrestrial transition zones with trees and herbaceous plants (Figure 1).

A statistical model of factors influencing variations in dissolved CO$_2$ concentrations was developed to evaluate the importance of inundation, vegetated habitats, planktonic productivity, DOC and hydrodynamics. Specifically, we expect: (1) CO$_2$ concentrations to vary seasonally and to increase as water depths and extent of inundation increase; (2) CO$_2$ concentrations in open water areas are influenced by vegetative habitats; and (3) more DOC and DOC of higher quality (lability) will lead to higher CO$_2$ concentrations. To further examine exchanges between vegetated areas and open waters, a three-dimensional hydrodynamic model was adapted to conditions on the floodplain. The results of our study contribute to understanding of controls of CO$_2$ concentrations in inland waters.

METHODS

Study Sites

Measurements were made in two parts of Lake Janauacá that differed in wind exposure, stratification and proximity of the open water to vegetated habitats: open lake (3° 22.6′ S, 60° 15.2′ W) and an embayment (3° 24.4′ S, 60° 14.8′ W) (Figure 1). Further description of the Janauacá floodplain is provided in Bonnet and others (2017), Amaral and others (2018, 2020) and in Supplementary Material.

Environmental Measurements

Sampling started near sunrise (~ 6 am) and was conducted at 4–6-h intervals with each site sampled at least three times over a 24-h period. At each site, open water was present at all times, and the presence and areal extent of floating plants and flooded forest habitats varied seasonally (Figure 2). Measurements of carbon dioxide partial pressure (pCO$_2$), together with environmental parameters including meteorological variables (wind speed and direction, relative humidity, photosynthetically available radiation (PAR) and air temperature), Secchi disk visibility and underwater profiles of PAR (indications of water clarity), vertical profiles of temperature and dissolved oxygen (DO), electrical conductance, pH, dissolved organic carbon (DOC), indices of colored dissolved organic matter (CDOM), chlorophyll-a (Chl-a), total nitrogen (TN), total phosphorus (TP) and total suspended sediments (TSS), were made on twenty occasions between August 2014 and September 2016, representing two hydrological years. Water for Chl-a, DOC, CDOM, TSS, TN and TP analyses was col-

lected at both stations from 0.5 m depth. CDOM indices include specific absorbance at 350 nm (a_{350}), ultraviolet absorbance at 254 nm (SUVA) and the slope ratio (SR). SUVA is negatively associated with microbial degradation and discriminates between labile and refractory DOC (Hansen and others 2016). SR is inversely related to DOC molecular weight and higher values represent proportionally more low molecular weight compounds (Helms and others 2008). The depth of active mixing was estimated as the depth from the near-surface temperature to the depth with an increase in temperature of 0.02 °C. Daily measurements of water levels, obtained from manual readings at two altimetric-referenced stage gauges (Bonnet and others 2017), were used to estimate ΔZ, which was the water level change over the 10 days before each sampling period. Methodological details are provided in Supplementary Materials.

On each sampling occasion, for a given aquatic habitat investigated over a 24-h period, pCO$_2$ profiles were measured using an off-axis integrated-cavity output spectrometer (Ultraportable Green-
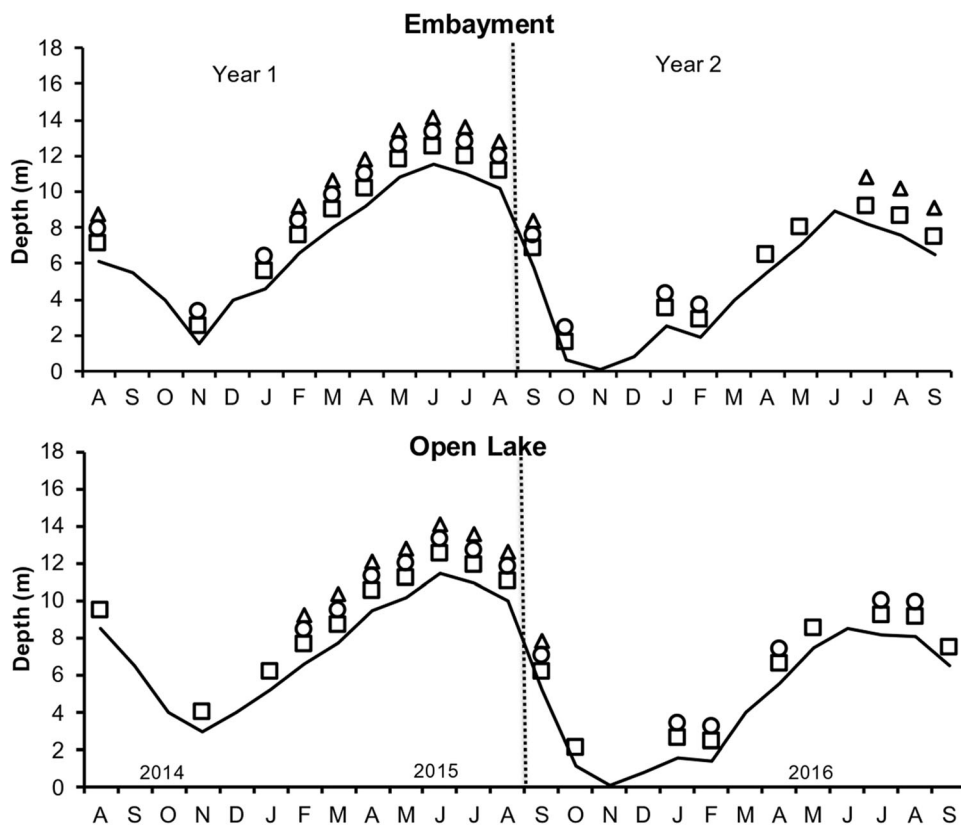

Figure 2. Measurement dates in open water (square), flooded forest (triangle) and floating herbaceous plant (circle) habitats and water depths at open water locations in lake and embayment from August 2014 to September 2016. Dashed lines separate hydrological years.

house Gas Analyzer—UGGA, Los Gatos Research) connected to a marble-type equilibrator (Frankignoulle and others 2001), through which lake water was pumped from near-surface (0.2–0.3 m), and from one-meter depth intervals to within 0.5–1 m of the bottom. Dissolved CO$_2$ concentrations were computed from pCO$_2$ in μatm (at atmospheric pressure of 1 atm) using Henry's constant computed from water temperature. Water-column concentrations were calculated by averaging the concentrations measured at all depths.

Herbaceous plant areas for the northern portion of Lake Janauacá were estimated from satellite imagery (Figure 1). Multispectral images (RapidEye Orthorectified Level 3A images acquired in August 2014, 2015 and 2016 with a spatial resolution of 6.5 m resampled to a 5-m grid and a high-resolution multispectral image (Apollo World View 2; August 2014) with 0.7 m resolution were used to manually classify floating plants, based on field observations and spectral characteristics. The high-resolution image covered an area of 25 km^2 that included the open lake and embayment sites. The areas of flooded forest and open water for each sampling campaign were estimated as described in Amaral and others (2020) and were used to calculate the ratio between open water and inundated forest areas.

Statistical analysis

We adopted a multiple-level statistical approach to analyze spatial variability of CO$_2$ concentrations at different temporal scales and in relation to environmental and landscape variables. First, we analyzed the overall differences in CO$_2$ concentrations between the embayment and lake sites, as well as changes per site in water-column concentrations at diel, seasonal and inter-annual scales. We compared concentrations between sites and day–night differences with paired t tests, and by one-way ANOVA when comparing more than one sampling campaign or hydrological period. We used two-way ANOVA to test differences between hydrological periods among different years. We used Tukey's HSD as a post hoc procedure that corrects alpha for multiple comparisons without losing statistical power.

Second, we calculated water-column CO$_2$ concentrations per campaign and per site to compare with environmental and landscape variables, averaged, if necessary, to obtain daily values. We grouped variables by terms expected to influence CO$_2$ concentrations:

$$CO_2 = \alpha \pm \beta_1 \text{ inundation} \pm \beta_2 \text{ productivity}$$
$$\pm \beta_3 \text{ DOC} \pm \beta_4 \text{ mixing} \pm \beta_5 \text{ other} \qquad (1)$$

The term called inundation includes the variables ΔZ, and the open water to flooded forest area ratio. The productivity term includes near-surface CO$_2$ concentration in herbaceous plant mats, Chl-a, nutrients (TN and TP), and light-related variables (Secchi depth, TSS and underwater attenuation of PAR). The DOC term includes the DOC concentration and its optical properties represented by SUVA, SR and a_{350}. The mixing term includes the depth of active mixing and wind speed. Finally, the term called other includes surface conductivity and temperature. As a first step, to select and reduce the variables to be included in the model to explain CO$_2$ variability, we tested the autocorrelation between variables associated with each of the terms using the $rcorr$ function in the package $Hmisc$. When autocorrelation ($p < 0.05$) between variables within a term occurred, we selected the variable with best theoretical or biological explanation (see "Results").

With the variables selected, we performed a further selection and averaging model procedure (Grueber and others 2011) with the goal to retain a set of models weighted by information theoretic criteria to account for model selection bias (Anderson 2008; Lukacs and others 2010). First, we used variance inflation factor analysis to identify collinear variables in the resulting model after step one, and a threshold of 5 was chosen to remove collinear variables, representing different terms in the model, which was called full model. Response and all predictor variables in the full model were standardized using the arm package (Gelman and Su 2018), a step for interpreting the parameter estimates after model averaging. From this model we generated a confidence set, using the "dredge" function available in the $MuMIn$ package (Barton and Barton 2018). We used the function "get.-models" from the $MuMIn$ package to obtain the top models within two units of DAICc of the "best" model (Grueber and others 2011). As a final step we used the "model.avg" function in R to estimate parameter coefficients in the confidence set, calculating conditional values using the mean of regression coefficients weighted by the AIC weight (wi) from each model including that variable (Gruner and others 2017). Graphs and statistical analyses were done using GraphPad Prism Version 7.01, and in R (R Core Development Team 2020).

Hydrodynamic Modeling

Modeling of the hydrodynamics of open water regions in lake and embayment was conducted using the three-dimensional coupled Hydrodynamic-Aquatic Ecosystem Model (AEM3D) (Hodges and Dallimore 2019). AEM3D is derived from the Estuary, Lake and Coastal Ocean Model (Hodges and others 2000) and uses a z-coordinate Cartesian grid allowing non-uniform spacing in three directions and solves the unsteady Reynolds-averaged Navier–Stokes equation under the Boussinesq approximation. Details about the AEM3D numerical schemes are provided by Hodges (2000). We incorporated an additional algorithm to account for differences in heating caused by floating plants in the embayment (Woodward and others 2017). In the lake, a numerical tracer, expressed as CO_2 concentration of 250 μM, was continuously introduced through the water column near fringing aquatic vegetation. In the embayment, a numerical tracer with CO_2 concentration of 235 μM was introduced continuously into the upper 0.3 m of water inside the mat of floating plants, where respiration is likely to be considerable. The goal was to track the mass transfer induced by wind-driven motions in the open lake and by differential heating and cooling between the floating plants and adjacent water in the embayment.

The inputs to the model include bathymetry, meteorological variables and temperature measured at the lake and water level change (as described above and in Supplementary Materials). The model was run with a 60-s time-step, 100 m × 100 m × 0.1 m grid in the lake and a 20 s time-step, 5 m × 5 m × 0.1 m grid in the embayment. We confirmed that the model simulated the diurnal stratification and nocturnal mixing in the open lake and embayment, surface temperature difference between inside and outside the floating plants in the embayment, and wind-driven basin-scale motions in the open lake by comparison with time-series temperature data.

RESULTS

Temporal and Spatial Differences in CO_2 Concentrations

Embayment Open Water

CO_2 concentrations in near-surface waters of the open water in the embayment varied from 3.0 μM (low water) to 430 μM (rising water) with a mean ± standard deviation of 183 ± 97 μM (Table S1). Water-column CO_2 concentrations varied from 4.1 to 485 μM with an overall mean of 285 ± 116 μM. Water-column CO_2 concentrations measured during rising water (313 ± 89 μM) were similar to values measured during high water (351 ± 46 μM), but values from both periods were higher than concentrations measured during falling (226 ± 144 μM) and low water (168 ± 119 μM) based on one-way ANOVA (F(3, 102) = 12.9, $p < 0.001$) (Table 1). During February 2016, an especially high water-column CO_2 concentration was obtained (485 μM) that coincided with the decomposition of herbaceous plants that grew during the previous low water period.

Lake Open Water

In the open water of the lake, near-surface CO_2 varied from 0.2 (low water) to 280 μM (high water), with a mean of 131 ± 83 μM (Table S1). Water-column CO_2 concentrations varied from 0.2 to 302 μM with an overall mean of 157 ± 91 μM. Water-column CO_2 concentrations during high water (245 ± 46 μM) were significantly higher than values during low (11 ± 13 μM), rising (146 ± 71 μM) and falling water (190 ± 55 μM) (Table 1). Concentrations during low water were lower than in other periods, and rising and falling water periods were different based on one-way ANOVA (F(3, 102) = 61.5, $p < 0.001$).

Overall, CO_2 concentrations averaged through the water column were greater than the values measured near the surface (0.2–0.3 m) (Paired t test, $t = 11.7$, $df = 205$, $p < 0.001$) for both open water sites (Figure 3).

CO_2 Concentrations in Vegetated Habitats

Near-surface CO_2 varied from 8.0 to 2050 μM, and CO_2 averaged water-column values from 25 to 2032 μM in herbaceous plant mats. The highest CO_2 was recorded when a *Paspalum repens* bed was decomposing during the low water in 2015 in the embayment; this value was judged an outlier and removed from further comparisons. Mean concentration (without the outlier and with both sites combined) was 240 ± 81 μM for near-surface values and 275 ± 77 μM for water-column CO_2. Water-column CO_2 values were lower during low water than other periods (F(3, 115) = 4.7, $p = 0.004$) (Table 1).

At flooded forest sites, near-surface CO_2 varied from 19 to 329 μM, and CO_2 averaged water-column values from 21 to 392 μM. Mean concentration was 155 ± 71 μM for near-surface values and 217 ± 78 μM for water-column CO_2. Water-column CO_2 values were higher (257 ± 47 μM) dur-

Table 1. Median and Number of Observations, Mean and ($\pm$) Standard Deviation, Maximum and Minimum Water-Column CO$_2$ Concentrations (μM) in Open Water and Herbaceous Plant Habitats in L. Janauacá at Each Site During Low Water (LW), Rising Water (RW), High Water (HW) and Falling Water (FW).

| Site	CO$_2$ water column (μM)							
	Open water				Herbaceous plants			
	LW	RW	HW	FW	LW	RW	HW	FW
Open lake								
Median	4/17	156/34	249/20	185/33	nd	234/30	277/17	243/9
Mean	11 $\pm$ 14	146 $\pm$ 71	245 $\pm$ 46	190 $\pm$ 54	nd	248 $\pm$ 82	271 $\pm$ 42	236 $\pm$ 73
Range	0.2/46	3.8/255	135/302	70/298	nd	25/370	205/373	134/352
Embayment								
Median	205/13	288/45	330/23	275/21	185/7	280/34	342/9	352/9
Mean	168 $\pm$ 119	313 $\pm$ 89	351 $\pm$ 46	226 $\pm$ 144	180 $\pm$ 55	304 $\pm$ 64	345 $\pm$ 27	311 $\pm$ 89
Range	4/352	192/485	249/452	11/428	91/256	226/450	306/389	169/396

nd means not determined because macrophytes were lacking
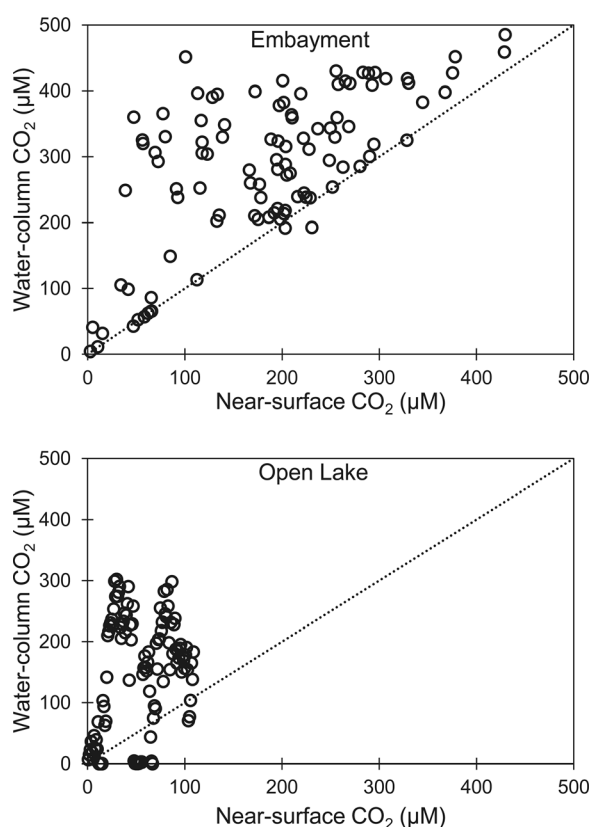
Figure 3. Differences between near-surface and water-column CO$_2$ concentrations measured at open water sites in embayment (left) and lake (right) in L. Janauacá. 1:1 line is dashed line.

ing high water than other periods (RW = 181 $\pm$ 60 μM, FW = 201 $\pm$ 97 μM) ($F_{(2, 72)}$ = 7.5, p = 0.001). A complete description of variations in near-surface water concentrations for flooded for-

est sites, including diel, seasonal and inter-annual variations is given in Amaral and others (2020).

Comparison Among Habitats and Sites

Mean near-surface CO$_2$ values in floating plant mats were higher than the mean values in the open water habitats: embayment ($F_{(3, 328)}$ = 30.6, $p < 0.001$) and open lake sites ($F_{(3, 328)}$ = 30.6, $p < 0.001$), respectively (Table S1). Open water values in the embayment were significantly higher than those measured in the open water of the lake (Table S1). In the embayment, open water, water-column CO$_2$ values were similar to those in herbaceous plant mats, and both were higher than mean concentrations measured in flooded forest habitats. Herbaceous plant and forest habitats fringing the open water of the lake had similar values, while open water had lower mean values than fringing vegetated sites ($F_{(5, 390)}$ = 27.6, $p < 0.001$). Water-column CO$_2$ values in the open water of the embayment were higher than the values measured in the same habitat in the lake ($F_{(5, 390)}$ = 27.6, $p < 0.001$) (Table 1).

Inter-annual Differences at Open Water Sites

Differences in water level between the two hydrological years are reflected in water-column CO$_2$ concentrations in open water environments (Figure 4A). When analyzing both open water sites together, the interaction between hydrological period and sampled year is statistically significant (two-way ANOVA, water column: $F_{(3, 198)}$ = 10.38; $p < 0.001$). Mean water-column CO$_2$ concentrations measured during the low water (118 $\pm$ 139 μM) and rising water (278 $\pm$ 132 μM)
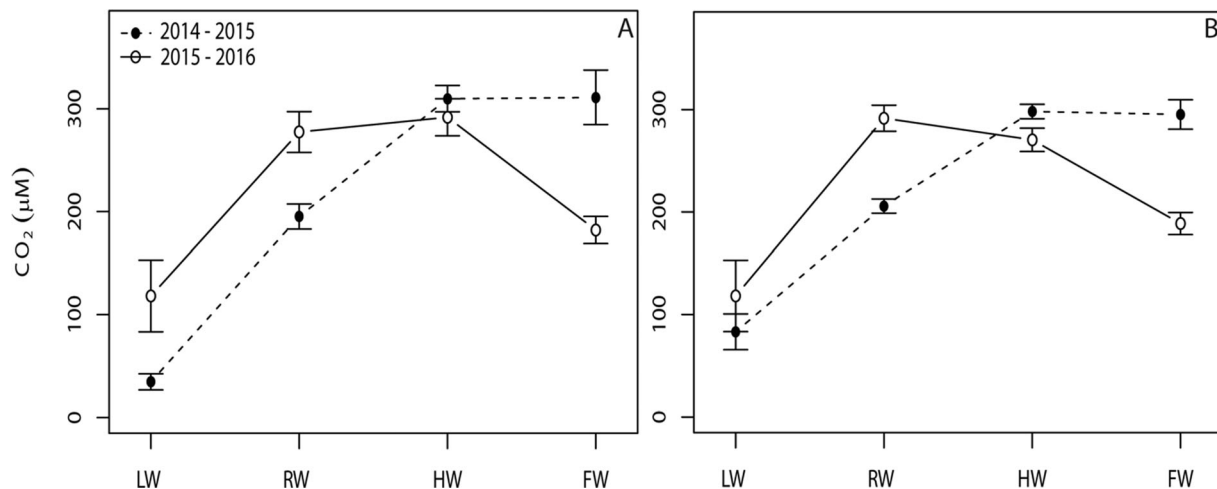
Figure 4. Water-column CO_2 concentrations for the **A** open water habitat, and **B** all habitats (forest, herbaceous plants and open water) combined during low water (LW), rising water (RW), high water (HW) and falling water (FW) of year one (2014–2015) black circles and year two (2015–2016) open circles. Dots represent mean values and error bars the standard deviations of the mean values.

of year two were higher than those in year one: more than 300% for LW (35 ± 29 μM) and 42% for RW (195 ± 72 μM) (Figure 4). In contrast, mean concentration measured during the falling water period of year one (311 ± 79 μM) was 70% higher than mean concentrations measured during year two (182 ± 89 μM), and mean high water concentrations were similar between years: Year $1 = 310 \pm 61$ μM and year $2 = 292 \pm 81$ μM. When comparing similar hydrological periods between years, rising and falling water periods were significantly different (Tukey's post hoc test, $p < 0.01$). Similar patterns between years are evident when all habitats are included (Figure 4B).

Diel Variability in CO_2

In open water sites of the embayment and lake, water-column CO_2 concentrations were variable over 24-h periods. The coefficient of variation (CV) varied from 3 to 88% for the embayment and from 2 to 102% in the lake, and the largest CVs were, in general, associated with high chlorophyll-a values (Table S3). In floating plant mats at both sites, less diel variability was observed compared to the open water and forested sites (Table S2).

Comparisons between day and night CO_2 concentrations were made for each campaign, per site for the open water habitats and were statistically different only in the lake site for water-column CO_2 values (paired t test, $t(15) = 2.8$, $p = 0.01$). At this site, mean CO_2 concentration was higher during the night compared to daytime.

Temporal and Spatial Differences in Environmental Conditions

Environmental Conditions at Open Water Sites

Environmental variables varied with water level. When water depths were shallow (1–5 m, low and rising water), Chl-a, TSS, DOC, temperature, DO, pH, underwater attenuation of PAR (Kd) and conductivity were, in general, higher compared to periods with greater water depths (6–12 m, high and falling water) (Tables S3 and S4). Chl-a, conductivity and near-surface DO concentrations were, in general, higher in the lake compared with the embayment, although values during high water were similar. In open water in the embayment, vertical gradients in temperature and DO developed during rising and falling water and resulted in an anoxic hypolimnion during the stratified period. In contrast, in open water in the lake vertical gradients with anoxic hypolimnetic waters were observed only during high water. At both sites, a shallow diurnal thermocline often occurred and varied as a function of wind speed and solar inputs. The wind speeds in the embayment were usually below the threshold of the anemometer (< 0.4 m s^{-1}) at night and early mornings and often higher in early afternoon (0.5–2.5 m s^{-1}). In the open lake, wind speeds between 2.5 and 5.0 m s^{-1} were common, and during occasional storms increased briefly up to 10 m s^{-1}. The actively mixing layer was deeper in the open lake compared to the embayment. In the open lake, this region of the upper water column averaged 1.2 and

1.7 m during low and rising water, respectively, and 2.1 and 2.6 m during high and falling water periods. In the embayment, it exceeded 1.0 m (reaching 1.5 m) only during falling water, while during low and high water it averaged 0.6 m, and during rising water averaged 0.9 m.

Inter-annual Changes in Herbaceous Plants

Areal coverage of herbaceous plants was different in the second year compared to the first year. The areal coverage estimate for the 25 km^2 quadrant (Figure 1) in 2016 (0.2 km^2) is about one-third of the estimate for 2015 (0.6 km^2) and half of the area estimated for 2014 (0.4 km^2). In the embayment, there were no herbaceous plants present during high and falling water periods at our sampling site in 2016, in contrast to 2014 and 2015.

Diel Variations in Temperature, DO and CO$_2$

Data from September 2015 illustrate typical diel variability of temperature, DO and CO$_2$ concentrations in herbaceous plant mats and open water of the embayment (Figure 5). As a result of high solar radiation, near-surface water temperature increased rapidly in the mats and in the open water, reaching 40 °C in near-surface water within the mat. Near-surface stratification also increased rapidly at both locations. Temperatures were 6 °C warmer in the plant mat than offshore, conditions that are conducive to flow of warmer water to open water (Figure 6). The vertical temperature gradient was 6 °C over 0.5 m in the plant mat, a condition that also contributed to horizontal temperature gradients. Cooling began as solar radiation decreased, and as a result, temperatures became isothermal in the upper 2 m. A seasonal thermocline was present below 2 m with undulations indicative of internal wave motions at both sites.

Dissolved oxygen was elevated with the largest vertical gradients when temperature stratification was strongest. Deeper depths had hypoxic or anoxic water. As the water cooled and stratification weakened, DO declined within the mats but increased mid-water column. The CO$_2$ profiles illustrate large differences in concentration through the water column, higher values under the mat during the stratified, daytime period, and high values in the upper water during the night in both habitats. The hydrodynamic simulations complement these measurements and illustrate when the patchy increases in concentration result from lateral intrusions (Figure 6).
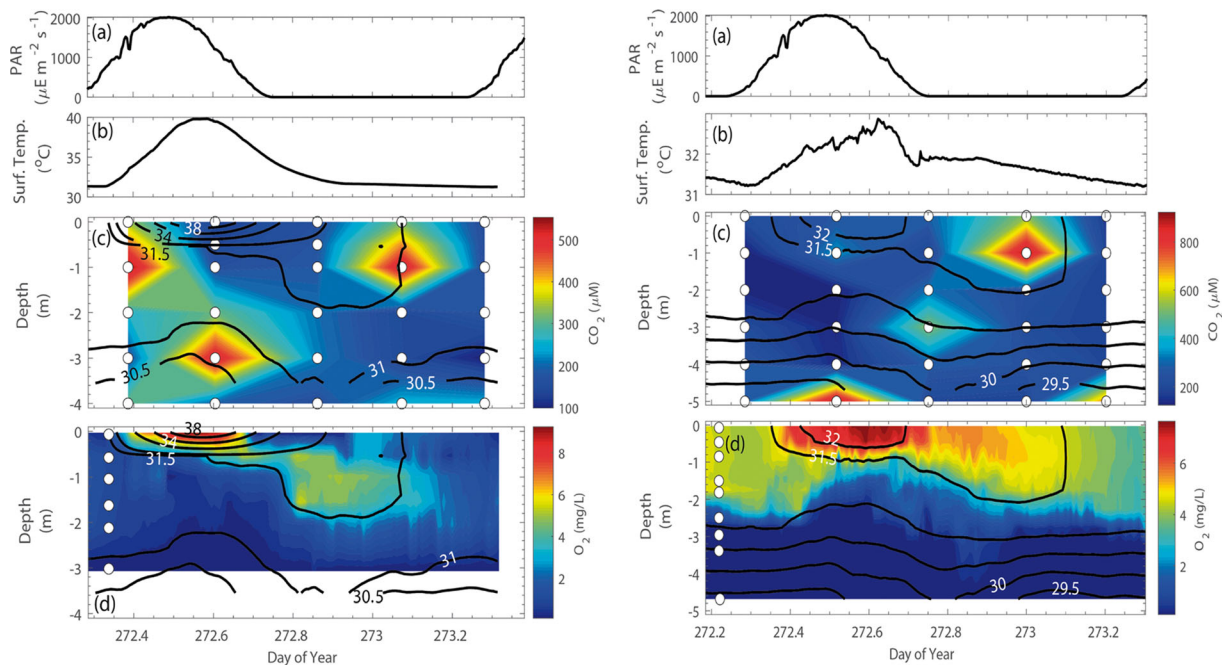

Figure 5. Diel variations during falling water (September 2015) in herbaceous plant mats (left) and open water (right) of embayment of L. Janauacá. Photosynthetically active radiation (PAR, **A**), surface temperature (0.05 m) (**B**), CO$_2$ (**C**) and dissolved oxygen (**D**) contours (colors) with white dots representing depths of measurements of CO$_2$ and position of dissolved oxygen sensors; black lines are isotherms based on thermistors (spaced 0.3–0.5 m over the top 2 m and 0.5–1 m over the other depths).
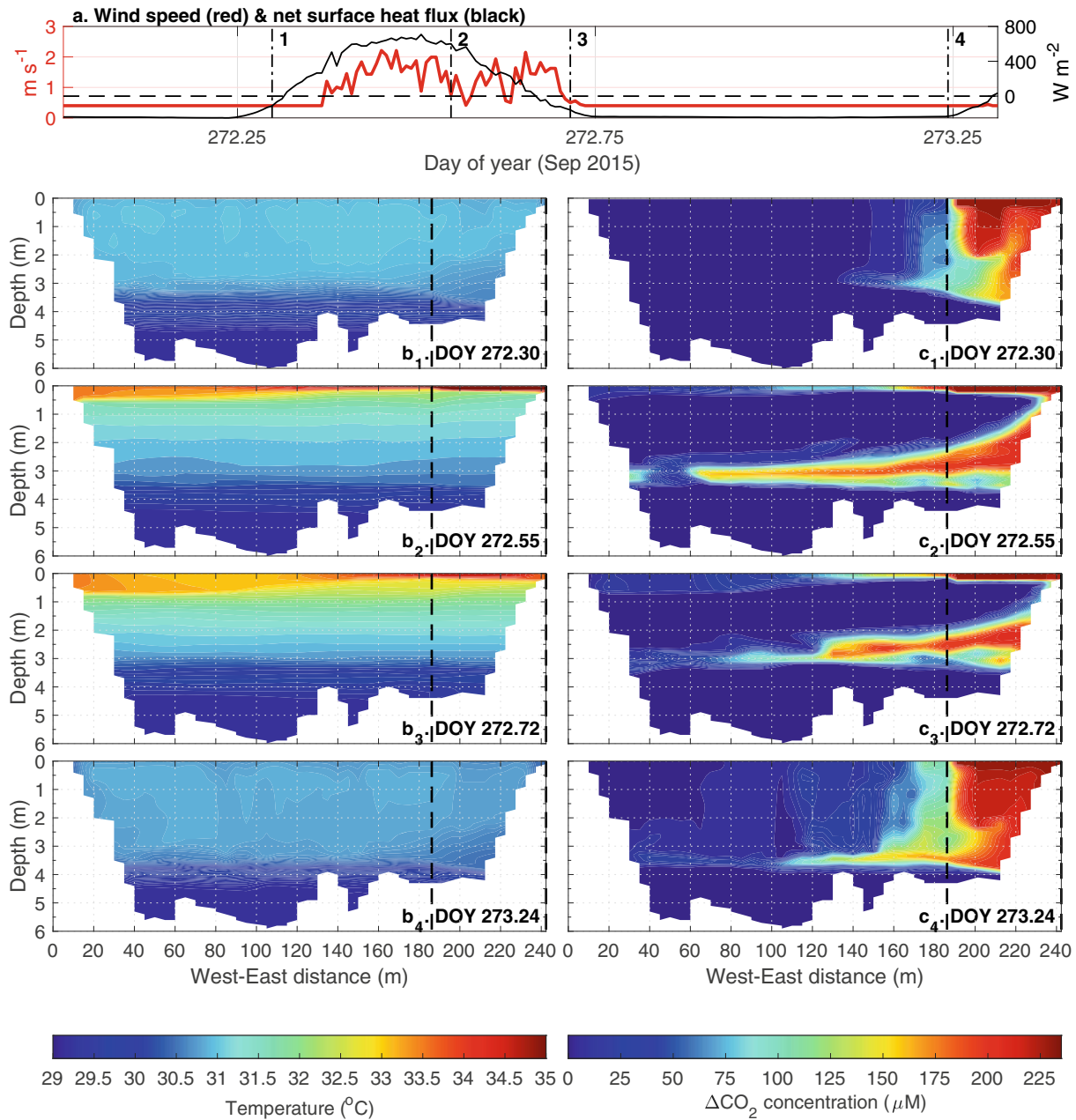
Figure 6. Cross sections illustrating hydrodynamic simulations over a diel cycle for the embayment. Wind speed and net surface heat flux (**A**) and snapshots of AEM3D simulated vertical profiles of temperature (**B**$_1$ to **B**$_4$) and tracer expressed as increases in CO_2 concentrations caused by dispersion of water with an estimated concentration of 235 μM from within the macrophyte mats (**C**$_1$ to **C**$_4$) at four different times marked by the numbered dash–dot lines in panel **A**. The black dashed lines mark the extent of the plant mat. A video for this hydrodynamic simulation can be seen at Supplementary Materials 2

Hydrodynamic Simulations

In the embayment, the modeled advection of the tracer away from the floating plants followed a diel cycle in four stages (Figure 6; Figure S4 and Supplementary Materials): (1) during the first two hours after sunrise (6:00 a.m. to 8:00 a.m.), surface

water continued to cool and wind speeds were negligible. With near-shore cooling, tracer, which had been added at 0.3 m, descended along the sloping boundary to a depth of 2–3 m. Then, on reaching a depth with comparable density, the tracer flowed offshore. This process is known as differential cooling. (2) From 8:00 am to 5:30 pm,

due to the considerable heating of water within the floating plant mats, tracer flowed from the mat to open water in the upper 0.3 m. With the increased stratification, and some wind, a three-layer flow was established, with that near the surface and at 2–3 m flowing offshore with the layer in between flowing in the opposite direction. The modeled results indicate that elevated concentrations of CO$_2$ could occur in a shallow, surface layer extending 30–40 m from the mat. Similarly, a plume with elevated CO$_2$ was found at 3 m that extended across the embayment. (3) During the hour before sunset (5:00 p.m. to 6:00 p.m.), when surface cooling had started and wind speed approached zero, the flow was reversed and, with the decline in the horizontal temperature gradient, the near-surface flow due to differential heating ceased. With cooling causing some mixing near the surface, the surface plume was dispersed. (4) After sunset and before sunrise the following day, cooling eroded the diurnal thermocline. Tracer outside the floating mat was mixed by penetrative convection, while tracer inside the mat again flowed downward and offshore. These descending plumes reached the seasonal thermocline. During these last two time periods, inputs of CO$_2$ from floating plant mats to open water were reduced near the surface, whereas the plume at $\sim$ 3 m extended further through the embayment (Figure S4). Flows such as these explain the intermittent increases of CO$_2$ observed above the seasonal thermocline in the embayment (Figure 5).

Simulated, near-surface, horizontal velocities within the plant mats were low (Figure S5; 0.001–0.004 m s^{-1}) and are similar to those measured with a warm-bead thermistor flow meter in a similar floating mat by Doyle (1991). In the open water of the embayment, simulated near-surface velocities of 0.01–0.04 m s^{-1} were also similar to those measured just outside the mat by Doyle.

In the open lake, movement of the tracer, analogous to the movement of CO$_2$, was moderated by both wind direction, temperature differences and internal wave motions, and exchange between the littoral and pelagic zones occurred at the surface and below with the depth of the flow dependent on wind direction (Figure 7; Figure S6). Despite the weak temperature gradient, the water column was stratified. Thus, upwelling of cooler water in the northern basin occurred when winds were northerly or easterly and downwelling when they shifted. Tracer injected along the northern margin during early morning, when temperatures were cooler inshore than offshore, descended during onshore flow and concomitant downwelling con-

ditions. As flow near the surface was toward the margin, flow in the lower water column was reversed and the plume moved offshore at depth. Such movement would transfer CO$_2$ offshore with the expectation that CO$_2$ concentrations would increase. Tracer injections when winds were from the north indicated northerly flow of the plume at the surface and more limited flow in the lower water column. When southerly winds that had been sustained for several hours ceased, the thermocline tilted in the opposite direction as surface water reversed direction. Thus, the tracer plume changed direction in both surficial and near-bottom waters (Figure 7b3, c3). Hence, potential inputs of CO$_2$ from fringing regions are sensitive to wind direction and associated water motions.

Here, we have simulated the pathway of flow from the northern edge. Given that fringing forest and floating macrophytes occur around the open water, CO$_2$ would be expected to be flowing from inshore regions to offshore from around the lake during the day. At night, the CO$_2$ which had accumulated to the upper water would be mixed vertically by penetrative convection.

Integration of CO$_2$ Patterns with Environmental Conditions

As the first step in statistical model development, we identified colinear variables within the terms of Eqn. (1). Actively mixing depth (AMLD) was selected as the mixing term, as it was shallow in the morning when winds tended to be light and deepened with increasing wind speed and with cooling at night. Near-surface CO$_2$ concentration in herbaceous plant mats (CO$_2$-MAC), Chl-*a*, and TN were selected as productivity terms. TP was correlated with TN and, therefore, not included in the model. Secchi depth was chosen as a proxy of water clarity as it correlated well with TSS and Kd, but was not correlated with the other productivity variables. The DOC term included DOC concentration as quantitative component (no correlations with CDOM—quality proxies), and SR as a DOC-quality variable, since it correlated or marginally correlated with the other CDOM parameters (SUVA and a$_{350}$). There was no correlation between variables representative of the inundation term, so both ΔZ and the open water to flooded forested area ratio (OW:forest area) were included in the model. Finally, temperature was chosen, as it correlates with specific conductance, an indicator of river or stream water, to represent the term called other.
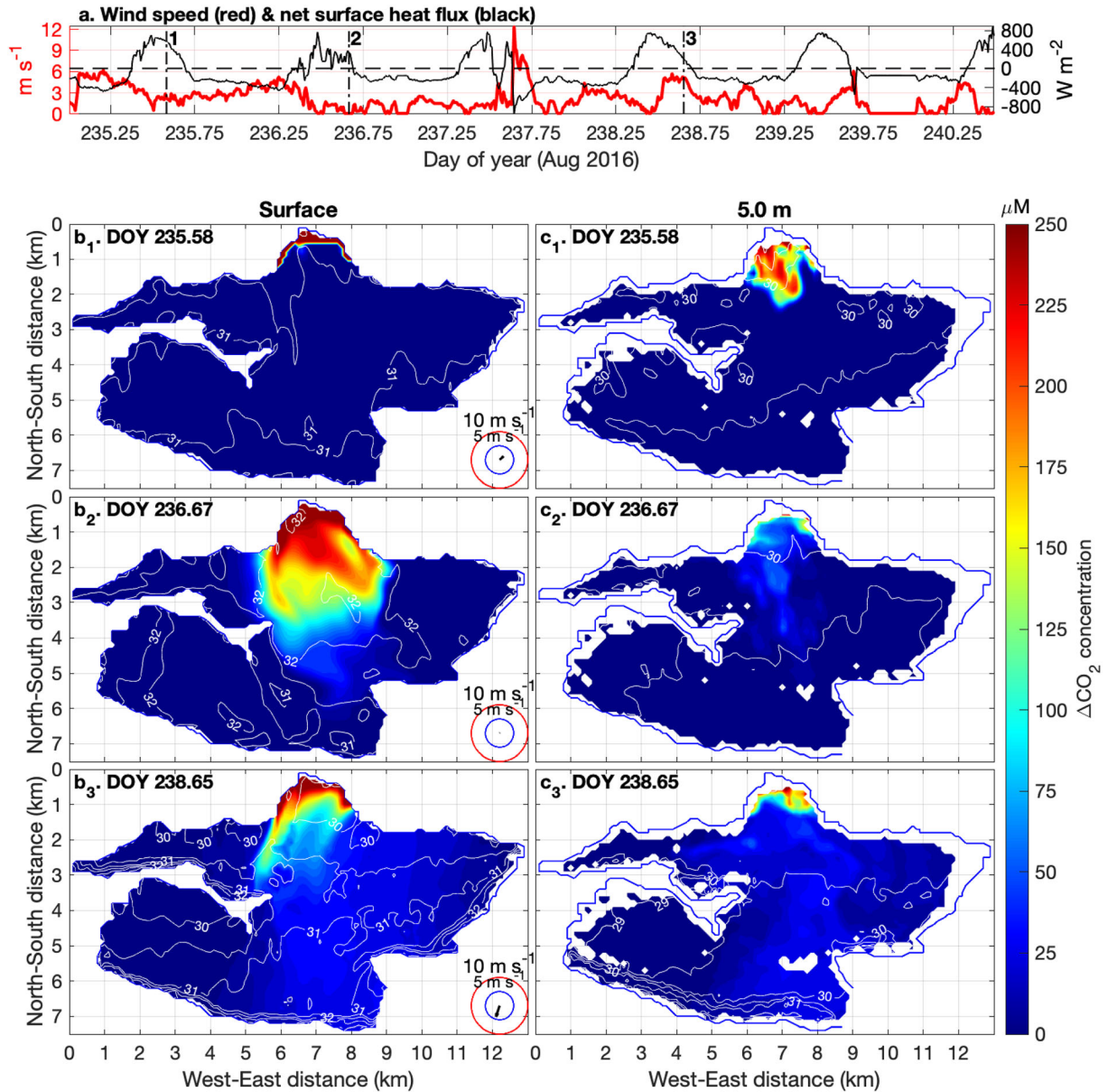
Figure 7. Hydrodynamic simulations for open lake illustrating movements of a plume of tracer as CO_2 viewed in plane-view at two depths. Meteorological conditions and water level as measured in August 2016. Wind speed and net surface heat flux indicating surface heating and cooling (**A**). Simulated tracer as increases in CO_2 concentration caused by dispersion of water with an estimated concentration of 250 μM within fringing vegetation across the domain at surface (**B₁** to **B₃**) and 5.0 m (**C₁** to **C₃**) at DOY 235.58, 236.672 and 238.65. White lines in each contour are the isotherms spaced at 0.5 °C. Arrows and circles at the lower right corner of the surface panels show the wind direction and speed.

The full model started with the ten selected variables, but OW:forest area and temperature were excluded from the model after the VIF correlation test. CO_2-MAC, Chl-*a*, Secchi depth and ΔZ were selected and distributed into three best models within 2.0 AIC units from the best model. The magnitude of the effect that each variable had on water-column CO_2 concentrations indicates that CO_2-MAC is the variable with the highest estimate

followed by Secchi depth, ΔZ and Chl-*a* (Figure 8). Hence, Eqn. (1) can be rewritten including variables present in the best models with their respective estimators:

$$CO_2 = \alpha + 0.18\,\Delta Z - 0.19\,\text{Chla} + 0.33\,\text{Secchi} + 0.69\,CO_2\,\text{MAC}. \qquad (2)$$
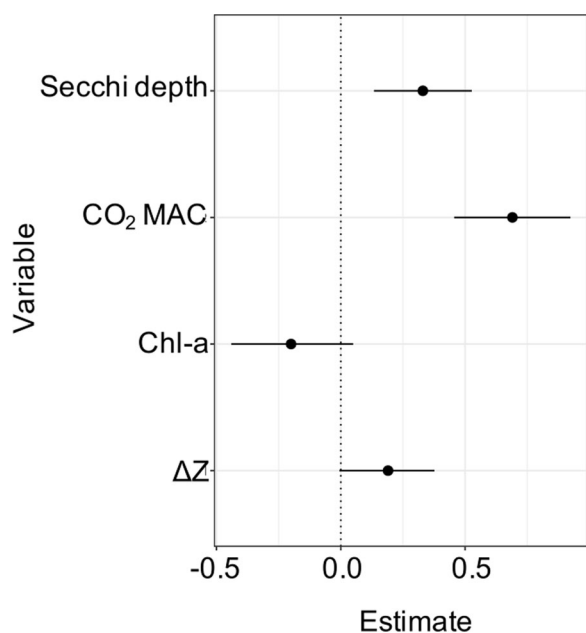
Figure 8. Estimates for regression slopes (± 95% confidence intervals, CIs) showing the magnitude and direction of the effects of different variables on water-column CO$_2$ concentrations within the eleven campaigns sampled between November 2014 and October 2015 on the Janauacá floodplain. Solid circles indicate the mean estimates and horizontal lines indicate confidence intervals. For significant variables, CIs do not cross the dotted line at zero.

DISCUSSION

Our findings elaborate and extend understanding of CO$_2$ in tropical lakes and floodplains with measurements and models covering the four hydrological phases. Measurements were obtained over diel cycles and in open water and vegetated habitats. The best statistical model of water-column CO$_2$ concentrations included terms representing inundation (ΔZ) and three terms related to primary productivity (planktonic chlorophyll-a, CO$_2$ associated with herbaceous plant mats, and transparency as indicated by Secchi depth). CO$_2$ associated with herbaceous plant mats had the strongest positive influence, while planktonic chlorophyll was less important and had a negative effect. While the statistical model considered several factors related to changes in CO$_2$ concentrations, the terms used to represent the factors do not include all the processes. Hence, other ecological and biogeochemical processes based on the relevant literature are combined with discussion of our results. The hydrodynamic modeling enhances understanding of specific physical processes influencing CO$_2$ dynamics. As will be discussed below,

our observations provide a new perspective on the active pipe hypothesis.

Herbaceous Plants as a Source of CO$_2$ to Open Waters in Floodplain Lakes

In Amazon floodplain lakes, a significant amount of CO$_2$ is derived from vegetated aquatic habitats and is transported by physical processes into open waters. This result contrasts with the emphasis on the supply and processing of terrestrial inputs by lakes and rivers as conceptualized and quantified in numerous lakes by the active pipe hypothesis (Cole and others 2007), suggested by Richey and others (2002) for the Amazon basin and incorporated into models of Amazon carbon cycling (Lauerwald and others 2017). The floating mats of herbaceous plants commonly found in Amazon floodplain lakes are predominantly highly productive C4 grasses (Piedade and others 1991; Junk and Piedade 1993; Engle and others 2008). These plants obtain CO$_2$ from the atmosphere and add almost all their organic carbon to the water during an annual growth and decomposition cycle. Engle and others (2008) estimated that loss rates per month of above- and below-water biomass ranged from 31 to 75%, amounting to 30–34 gC m^{-2} d^{-1}. Almost all the carbon in this plant biomass is decomposed rapidly in the water and surficial sediments (Furch and Junk 1997; Mortillaro and others 2016) releasing dissolved CO$_2$ and CH$_4$.

The results from stable isotopic analyses support the idea of the importance of herbaceous aquatic plants to CO$_2$ concentrations in floodplain lakes. Quay and others (1992) evaluated δ^{13}C values in different C fractions sampled on an 1800 km transect along the Solimões/Amazon River, including its main tributaries and a few floodplain sites, and suggested that about 40% of the respired organic carbon was derived from C4 herbaceous plants. In a central Amazon floodplain lake, Waichman (1996) compared the δ^{13}C value of CO$_2$ produced by bacterioplankton, incubated in filtered water sampled from open water, flooded forest and floating meadows to the plants in an Amazon floodplain lake in order to identify the autotrophic carbon source for these organisms. She found good agreement between the δ^{13}C values of the CO$_2$ produced and that of C4 herbaceous plants and concluded that bacterioplankton living in floating plant mats and flooded forests derived 90% of their carbon from C4 plants while those in open water environments derived 73% of their carbon from this source.

Respiration by the submerged roots and the periphyton community associated with the roots likely contribute to the high CO_2 concentrations within floating plant mats. The upper 0.5 m or so under floating plants is a mixture of roots, stems and leaves, all of which are substrata for epiphytic bacteria, algae and a diverse epifauna (Engle and Melack 1989). For example, in floating *Paspalum repens* mats in a central Amazon floodplain lake the roots represented approximately 11–48 gC m^{-2}, and attached periphyton 8.0–17 gC m^{-2} over a growing season (Engle and Melack 1993). Moreover, the organic matter produced by the periphyton is of higher quality for grazers than the plant material.

Doyle (1991) measured rates of photosynthesis and respiration of periphyton and associated roots in chambers deployed in situ with natural light and flow conditions. Autotrophic growth was limited to a shallow euphotic zone (often < 0.2 m). Doyle estimated the portion of respiration by root tissue to vary from 5.0 to 25% of the total respiration of the root plus periphyton depending on the size and colonization of the roots. To convert dissolved oxygen-based measurements of respiration to carbon, Doyle determined the ratio of moles of CO_2 produced to moles of O_2 consumed to be 0.8. Monthly rates of respiration, using his preferred extrapolation method, were calculated to vary from approximately 2.0 to 59 gC m^{-2} month^{-1} with an average of 33 gC m^{-2} month^{-1}. If converted to a daily rate and distributed in the upper 0.5 m of water, an average daily increase in CO_2 of about 200 μM would result. Another estimate of the total respiration associated with *P. repens* roots and periphyton is indicated by the night-time decline of DO within bags with a root cluster and periphyton from an average of 3.4–1.2 mg L^{-1} (Engle and Melack 1993). If converted to CO_2 using Doyle's ratio, 55 μM would be produced during the night.

Our measurements, statistical analysis and hydrodynamic modeling indicate that waters with elevated concentrations of dissolved gases can be mixed or advected from vegetated habitats to open water. Several physical processes can cause lateral and vertical motions that can link benthic, pelagic and littoral habitats (MacIntyre and Melack 1995). Floating mats of vascular plants can reduce solar radiation reaching into the water, resulting in cooler water under the mats but warmer near-surface water compared to open water and causing temperatures differentials and advective motions (Coates and Ferris 1994). As solar radiation declines in the day and is absent at night, water near the surface cools inducing vertical mixing of the water column by penetrative convection (Augusto-Silva and others 2019). This mixing brings dissolved gases which had been transported at depth by differential cooling in embayments (Figure 6) to the surface where they can evade to the atmosphere.

In open waters, stratification supports internal waves such that the thermocline up- and downwells with changes in wind speed and direction. These processes can bring high concentrations of CO_2 offshore to near the surface when winds flow offshore and to the lower water column when winds flow onshore. The circulation within the downwelled mixed layer is similar to that described by Mortimer (1952) in that surface water flows toward shore and that of the base of the mixed layer flows offshore. Thus, internal wave mediated flows transport dissolved gases either offshore near the surface or onshore to the lower water column. Nocturnal cooling or strong wind events can entrain waters with higher CO_2 concentrations from the lower water column increasing values in the upper water. When concentrations of CO_2 are elevated near the surface, evasion to the atmosphere is enhanced (Amaral and others 2020).

Inter-annual Variations of Herbaceous Plants and Impacts on CO_2 Concentrations

Year-to-year differences in plant growth and decay moderates CO_2 concentrations. These processes depend on the duration of low water. Higher CO_2 concentrations were observed in high and falling periods of the first year compared to the second year of our study (Figure 4). Exceptionally low water levels in 2015, caused by a regional, extended drought, possibly related to an El Niño event (Jiménez-Muñoz and others 2016), led to the mortality of floating *Paspalum repens* mats, and the emergence of large areas of exposed lake bottom on which *Luziola spruceana* and *Oryza rufipogon* grew (Amaral and others 2018; Rodrigo Nunes, personal communication). When water levels rose in January and February 2016, these areas were inundated, and *L. spruceana* senesced and decomposed. When water levels reached $\sim$ 5 m (March–April), *O. rufipogon* also senesced and decomposed. The mortality and decomposition of these plants were likely the cause of higher CO_2 during the rising water of year two compared to the year one, at both sites, as well as the atypically high CO_2 in the embayment during the low water period of year two (Table 1 and Table S1). Few floating plants occurred during the high and falling periods of 2016 in the embayment, which may have con-

tributed to the lower CO$_2$ values in the embayment during these periods when compared to similar periods in 2015, when floating plants were present (Figure 4). Areal coverage of floating herbaceous plant estimated by remote sensing for the 25 km^2 quadrant in 2016 was one-third of the estimate for a similar period in 2015.

Variations in Environmental Conditions, Their Impact on CO$_2$ Concentrations and Alternative Sources of CO$_2$ in Floodplain Lakes

In open waters, especially during low water, high chlorophyll-*a* concentrations are often observed in Amazon floodplain lakes (Tables S3 and S4; Barbosa and others 2010; Forsberg and others 2017a). The higher diel CV of CO$_2$ concentrations recorded during rising and low water is likely related to diel variations in plankton metabolism. Occasionally, under-saturation of CO$_2$ can occur in Amazon floodplain lakes during periods with abundant phytoplankton during daytime (Abril and others 2014; Amaral and others 2018). At night, CO$_2$ concentrations increase due to plankton respiration. These dynamics are evident in the day–night differences observed in the open lake. The inverse relationship between Chl-*a* and CO$_2$ concentrations, represented in the statistical model (equation 2), and commonly associated with pelagic primary production is likely to be the cause of lower CO$_2$ during the low and rising water period.

Several other variables were important in the model. Secchi depth was a positive term in the model. Reduced transparency is associated with sediment suspension during periods of low water and river inflows, and with abundant phytoplankton, especially in the open lake, that led to reduced CO$_2$. Conversely, increases in water transparency and water-column CO$_2$ in the embayment are likely related to stratified conditions, as CO$_2$ accumulated below the seasonal thermocline. Amaral and others (2018) provide an example of higher CO$_2$ concentrations in deeper water compared to upper water in both the main lake and embayment during a stratified period. During periods of falling water levels, as indicated by Δz, CO$_2$ enriched waters from the hypolimnion are likely to mix through the water column.

To further examine the relations between CO$_2$ concentrations and vertical mixing, we compared the ratio between near-surface and water column averaged CO$_2$ concentrations and the depth of the actively mixing layer. As mixing increased, differences between near-surface and water column averaged CO$_2$ concentrations, decreased, i.e., increased vertical mixing reduced vertical variability of CO$_2$ concentrations.

The metabolism of the plankton community is another source of variability in CO$_2$ concentrations in Amazon floodplain lakes (Richey and others 1988). Amaral and others (2018) reported rates of plankton respiration in Lake Janauacá of 97 µmoles CO$_2$ L^{-1} d^{-1} in the lake and 56 µmoles CO$_2$ L^{-1} d^{-1} in the embayment. Methane oxidation is also a planktonic source of CO$_2$; based on average rates of methane oxidation in Lake Janauacá, $\sim$ 2.0 µmoles CO$_2$ L^{-1} d^{-1} could be generated (Barbosa and others 2018).

The sediments of floodplain lakes sequestered some organic carbon and release CO$_2$ to the overlying water as a portion of the sedimented carbon is metabolized (Smith and others 2003). Using a simple model of diagenesis for two small Amazon lakes, Devol and others (1984) estimated 6.0 and 24 mmol m^{-2} d^{-1} of carbon was oxidized. Using submerged chambers, Smith-Morrill (1987) measured dissolved oxygen uptake during periods when the near-bottom waters were aerobic of 50 mmol m^{-2} d^{-1}. Under stratified conditions with anoxic bottom waters, carbon efflux from sediments estimated from efflux of ammonium and the C:N ratio in the sediments varied from 55 to 200 mmol m^{-2} d^{-1}.

CO$_2$ concentration is known to covary with DOC concentration across different lakes (Sobek and others 2005; Lapierre and del Giorgio 2012), and the relation is often interpreted to result from inter-lake variations in allochthonous organic and possibly simultaneous inorganic carbon inputs. However, within our single system (Lake Janauacá), we did not find a significant correlation between CO$_2$ and DOC concentrations (Pearson's correlation $p = 0.15$, $r^2 = 0.06$). This was consistent with the results of Waichmann (1996) who found the CO$_2$ liberated by bacterioplankton and the measurable DOC pool to be isotopically distinct. She suggested that two DOC pools existed in this system, a labile pool derived predominantly from C4 plants that is rapidly transformed into CO$_2$ and a more refractory pool derived predominantly from C3 plants that accumulates in the water column. That SUVA, an indicator of CDOM aromaticity, often associated with refractory terrestrial carbon (Weishaar and others 2003), was negatively correlated with CO$_2$ concentrations ($p = 0.12$, $r^2 = -0.29$) supports this argument. The highest SUVA values (> 5) occurred during low and rising water periods (Figure S1), when waters on the floodplain contain relatively more water from their local drainage

(Bonnet and others 2017). Furthermore, DOC in dry soils is likely to be mobilized by inundation (Melo and others 2019; Silva and others 2020), leading to high SUVA values measured during rising water. SR, with lower values indicating a CDOM of high molecular weight (Helms and others 2008), likely associated with DOC of terrestrial origin, had the lowest values during high water (Figure S1) and was low during early rising water. The CDOM parameters suggest a period of relatively high terrestrial inputs during early rising water, and of the importance of inputs during higher water periods. This inference is supported by CDOM parallel factor analysis (Melo and others 2019). Further research is needed to evaluate the importance of terrestrial inputs and possible priming effects on DOC removal and CO_2 production in floodplain lakes (Ward and others 2013).

In addition to movements of CO_2 within the Janauacá floodplain, inputs of water from local seepage and runoff and the Solimões River can introduce CO_2 and influence the variations in concentration observed. A water balance model and tracing of water with electrical conductance by Bonnet and others (2017) demonstrated large spatial and seasonal variations in the contributions of water from the different sources, and a water retention time in the lake from 27 to 71 days. Further evidence of the complexity of the water motions is provided by an application of a two-dimensional hydrological–hydrodynamic model that revealed heterogeneities in water velocities throughout the floodplain and how inputs from the Solimões River and local runoff influenced circulation patterns within the lake (Pinel and others 2020). During our study, concentrations of CO_2 in water at the southern end of the lake, at times with strong influence by local runoff and seepage, averaged 175 µM, and in the channel linking the lake to the Solimões River averaged 88 µM during periods of inflow with low floodplain influence. These values are less than most values measured in herbaceous plant mats and flooded forests, reinforcing the importance of aquatic vegetative habitats as sources of dissolved CO_2, in relation to other potential sources on the floodplain.

Implications Associated with Environmental Changes

Major changes in the discharge and flooding patterns of Amazon tributaries during the next 50 years are predicted due to anthropogenic climate change, with shallower water and reductions in inundation extent expected for most of the central Amazon (Sorribas and others 2016). Our study indicates likely expected outcomes. When exposed, lake sediments favor growth of herbaceous plants and when flooded by rising water, the plants decay and release CO_2 that can be emitted to the atmosphere. Our observations of DO depletion when the herbaceous plants were flooded and decaying support this interpretation. Furthermore, CH_4 concentrations in open waters of the Janauacá floodplain at this time were nearly 10 times higher than concentrations measured during the previous year during rising water (Barbosa and others 2020). Thus, multiple lines of evidence point to increased concentrations of CO_2 during rising water under regional droughts.

A complex set of metabolic pathways would moderate the carbon balance during extended low water periods on floodplains. Although CO_2 concentrations and outgassing rates can increase as a result of the decay of inundated rooted herbaceous plants, this carbon is likely to be largely balanced by photosynthetic uptake by these plants (Amaral and others 2018). However, since a portion of this organic carbon is transformed to CH_4, the emission of CH_4 will contribute to atmospheric warming. In addition, the conditions observed during the extended low water period emphasize the importance of the aquatic-terrestrial transition zone to the production and fate of organic matter (Kayler and others 2019).

The absence of floating herbaceous plants in the embayment during the high and falling water period of 2016 is likely associated with fires set by local residents during the prolonged low water period in early 2016. The fires may have affected the seed bank of *Paspalum repens*. Management actions should attempt to reduce the impact of slash and burn practices, especially under drought and extended low water conditions in order to preserve herbaceous and forest habitats. These conditions would also favor loss of sediments to the river, especially in floodplain areas that are susceptible to turbulence and water currents, with the potential to affect the establishment and regrowth of herbaceous species in these areas (Piedade and others 2010). The reduced presence of *P. repens* may also reflect the direct negative impact of the prolonged low water period on seed and rhizome survival, an effect which is expected to worsen with anthropogenic climate change (Sorribas and others 2016).

The building of dams on large Andean tributaries of the Amazon River will cause changes that may further moderate the carbon balance in the floodplain. The potential impacts of these dams include

reduced supplies of sediments, phosphorus and nitrogen to the lowland floodplains, with probable negative consequences for aquatic productivity, and changes in the timing and magnitude of seasonal flooding below dams which is expected to degrade flooded forests (Forsberg and others 2017b). These changes will modify the concentrations and emissions of CO$_2$ in floodplain environments. Strategic, basin-wide planning and the use of alternative energy sources could optimize energy production and minimize environmental impacts (Almeida and others 2019).

CONCLUSIONS

We demonstrated metabolic processes in floating herbaceous plants are a key driver of CO$_2$ variability in Amazonian floodplains. The influence of floating herbaceous plants exceeded that from changes in water level, pointing to within lake processes modifying the active pipe hypothesis. That is, respiration, production and decay of these plants were a major contributor to concentrations of CO$_2$, more so than water flowing in from the river or catchment. Physical processes transferred the CO$_2$ produced in near-shore regions to offshore locations with greater wind exposure where rates of evasion could be more rapid. We also found consistent differences in CO$_2$ dynamics between embayments and open lake portions of a floodplain system. In short, we have provided evidence for (1) aquatic herbaceous plants fringing floodplain lakes as sources of dissolved CO$_2$ to the open waters; (2) that CO$_2$ concentrations are higher in embayments particularly when stratified during high water in comparison with an open lake where mixing penetrated to deeper depth and facilitated evasion, thus water-column stratification and mixing are a source of CO$_2$ variability; (3) that diel differences in stratification and lateral movements of water alter CO$_2$ concentrations and can increase concentrations offshore; (4) that CO$_2$ concentrations were higher during periods with deeper water and larger areas of inundation; (5) that inter-annual differences in CO$_2$ concentrations were associated with changes in abundance of herbaceous plants and were affected by extended low water periods; and (6) how seasonally changing water levels and transparency interact with vertical mixing to alter CO$_2$. Our statistical model successfully incorporated variables to represent vegetation, inundation and vertical mixing as sources of variability in CO$_2$ concentrations.

Declarations

Conflict of interest
The authors declare that they have no conflict of interest.

REFERENCES

Abril G, Borges AV. 2019. Ideas and perspectives: Carbon leaks from flooded land: do we need to replumb the inland water active pipe? Biogeosciences 16:769–784.

Abril G, Martinez J-M, Artigas LF, Moreira-Turcq P, Benedetti MF, Vidal L, Meziane T, Kim J-H, Bernardes MC, Savoye N, Deborde J, Souza EL, Albéric P, Landim de Souza MF, Roland F. 2014. Amazon River carbon dioxide outgassing fuelled by wetlands. Nature 505:395–398.

Almeida RM, Shi Q, Gomes-Selman JM, Angarita H, Barros N, Forsberg BR, García-Villacorta R, Hamilton SK, Melack JM, Montoya M, Perez G, Sethi SA, Gomes CP, Flecker AS. 2019. Reducing the greenhouse gas footprint of Amazon hydropower with optimal dam planning. Nature Communications 10:4281. https://doi.org/10.1038/s41467-019-12179-5.

Amaral JHF, Borges AV, Melack JM, Sarmento H, Barbosa PM, Kasper D, de Melo ML, De Fex-Wolf D, da Silva JS, Forsberg BR. 2018. Influence of plankton metabolism and mixing depth on CO_2 dynamics in an Amazon floodplain lake. Science of the Total Environment 630:1381–1393.

Amaral JHF, Farjalla VF, Melack JM, Kasper D, Scofield V, Barbosa PM, Forsberg BR. 2019. Seasonal and spatial variability of CO_2 in aquatic environments of the central lowland Amazon basin. Biogeochemistry 143:133–149.

Amaral JHF, Melack JM, Barbosa PM, MacIntyre S, Kasper D, Cortés A, Silva TSF, Nunes de Sousa R, Forsberg BR. 2020. Carbon dioxide fluxes to the atmosphere from waters within flooded forests in the Amazon basin. Journal of Geophysical Research: Biogeosciences 125:e02019JG005293. https://doi.org/10.1029/2019JG005293.

Anderson, DR. 2008. Model based inference in the life sciences: a primer on evidence. Springer Science & Business Media

Augusto-Silva PB, MacIntyre S, de Moraes Rudorff C, Cortés A, Melack JM. 2019. Stratification and mixing in large floodplain lakes along the lower Amazon River. Journal of Great Lakes Research 45:61–72.

Barbosa CCF, de Moraes Novo EML, Melack JM, Gastil-Buhl M, Filho WP. 2010. Geospatial analysis of spatiotemporal patterns of pH, total suspended sediment and chlorophyll-a on the Amazon floodplain. Limnology 11:155–166.

Barbosa PM, Amaral JHF, Melack JM, Farjalla VF, da Silva JS, Forsberg BR. 2018. High rates of methane oxidation in an Amazon floodplain lake. Biogeochemistry 137:351–365.

Barbosa PM, Melack JM, Amaral JHF, MacIntyre S, Kasper D, Cortés A, Farjalla VF, Forsberg BR. 2020. Dissolved methane concentrations and fluxes to the atmosphere from a tropical floodplain lake. Biogeochemistry 148:129–151.

Barton K, Barton MK. 2018. Package 'MuMIn.' Version 1:18.

Bonnet M-P, Pinel S, Garnier J, Bois J, Resende Boaventura G, Seyler P, Motta Marques D. 2017. Amazonian floodplain water balance based on modelling and analyses of hydrologic and electrical conductivity data. Hydrological Processes 31:1702–1718.

Coates MJ, Ferris J. 1994. The radiatively driven natural convection beneath a floating plant layer. Limnology and Oceanography 39:1186–1194.

Cole JJ, Prairie YT, Caraco NF, McDowell WH, Tranvik LJ, Striegl RG, Duarte CM, Kortelainen P, Downing JA, Middelburg JJ, Melack JM. 2007. Plumbing the global carbon cycle: Integrating inland waters into the terrestrial carbon budget. Ecosystems 10:172–185.

Devol AH, Zaret TM, Forsberg BR. 1984. Sedimentary organic matter diagenesis and its relation to the carbon budget of tropical Amazon floodplain lakes. Verhandlungen Internationale Vereinigen Limnologie 22:1299–1304.

Doyle, RD. 1991. Primary production and nitrogen cycling within the periphyton community associated with emergent aquatic macrophytes in an Amazon floodplain lake. Ph.D. Thesis. University of Maryland. 269 p.

Drake TW, Raymond PA, Spencer RGM. 2018. Terrestrial carbon inputs to inland waters: A current synthesis of estimates and uncertainty: Terrestrial carbon inputs to inland waters. Limnology and Oceanography 3:132–142.

Engle DL, Melack JM. 1989. Floating meadow epiphyton: biological and chemical features of epiphytic material in an Amazon floodplain lake. Freshwater Biology 22:479–494.

Engle DL, Melack JM. 1993. Consequences of riverine flooding for seston and the periphyton of floating meadows in an Amazon floodplain lake. Limnology and Oceanography 38:1500–1520.

Engle DL, Melack JM, Doyle RD, Fisher TR. 2008. High rates of net primary production and turnover of floating grasses on the Amazon floodplain: implications for aquatic respiration and regional CO_2 flux. Global Change Biology 14:369–381.

Forsberg BR, Melack JM, Richey JE, Pimentel TP. 2017a. Regional and seasonal variability in planktonic photosynthesis and planktonic community respiration in Amazon floodplain lakes. Hydrobiologia 800:187–206.

Forsberg BR, Dunne T, Melack JM, Venticinque E, Goulding EM, Barthem R, Paiva RCD, Sorribas MV, da Silva-Júnior UL, Weisser S. 2017b. Potential impact of new Andean dams on the Amazon fluvial ecosystems. PLoS One 12(8):e0182254.

Frankignoulle M, Borges A, Biondo R. 2001. A new design of equilibrator to monitor carbon dioxide in highly dynamic and turbid environments. Water Research 35:1344–1347.

Furch K, Junk WJ. 1997. The chemical composition, food value and decomposition of herbaceous plants, leaves, and leaf litter of the flooded forests. In: Junk WJ, Ed. Central Amazon floodplain. Ecological Studies, . Berlin: Springer. pp 187–206.

Gelman A, Su Y-S. 2018. arm: data analysis using regression and multilevel/hierarchical models. R package version 1.10-1. https://CRAN.R-project.org/package=arm.

Grueber CE, Nakagawa S, Laws RJ, Jamieson IG. 2011. Multimodel inference in ecology and evolution: challenges and solutions: Multimodel inference. Journal of Evolutionary Biology 24:699–711.

Gruner DS, Bracken MES, Berger SA, Eriksson BK, Gamfeldt L, Matthiessen B, Moorthi S, Sommer U, Hillebrand H. 2017. Effects of experimental warming on biodiversity depend on ecosystem type and local species composition. Oikos 126:8–17.

Hansen AM, Kraus TEC, Pellerin BA, Fleck JA, Downing BD, Bergamaschi BA. 2016. Optical properties of dissolved organic matter (DOM): Effects of biological and photolytic degradation. Limnology and Oceanography 61:1015–1032.

Helms JR, Stubbins A, Ritchie JD, Minor EC, Kieber DJ, Mopper K. 2008. Absorption spectral slopes and slope ratios as indicators of molecular weight, source, and photobleaching of chromophoric dissolved organic matter. Limnology and Oceanography 53:955–969.

Hess LL, Melack JM, Affonso AG, Barbosa C, Gastil-Buhl M, Novo EMLM. 2015. Wetlands of the lowland Amazon basin: extent, vegetative cover, and dual-season inundated area as mapped with JERS-1 synthetic aperture radar. Wetlands 35:745–756.

Hodges, BR. 2000. Numerical Techniques in CWR-ELCOM (code release v.1). Nedlands, Australia: The University of Western Australia, Center for Water Research. 37p.

Hodges BR, Dallimore C. 2019. Aquatic ecosystem model: AEM3D, user manual. Docklands, Australia: Hydronumerics.

Hodges BR, Imberger J, Saggio A, Winters KB. 2000. Modeling basin-scale internal waves in a stratified lake. Limnology and Oceanography 45:1603–1620.

Jiménez-Muñoz JC, Mattar C, Barichivich J, Santamaría-Artigas A, Takahashi K, Malhi Y, Sobrino JA, van der Schrier G. 2016. Record-breaking warming and extreme drought in the Amazon rainforest during the course of El Niño 2015–2016. Scientific Report 6:33130.

Johnson MS, Lehmann J, Riha SJ, Krusche AV, Richey JE, Ometto JPHB, Couto EG. 2008. CO$_2$ efflux from Amazonian headwater streams represents a significant fate for deep soil respiration. Geophysical Research Letters 35:L17401.

Junk WJ, Bayley PB, Sparks RE. 1989. The flood pulse concept in river-floodplain systems. Canadian Special Publication of Fisheries and Aquatic Sciences 106:110–127.

Junk WJ, Piedade MTF. 1993. Biomass and primary-production of herbaceous plant communities in the Amazon floodplain. Hydrobiologia 263:155–162.

Junk WJ, Piedade MTF, Wittmann F, Schöngart J, Parolin P, Eds. 2010. Amazonian floodplain forests: ecophysiology, biodiversity and sustainable management. Dordrecht (Netherlands), New York: Springer.

Kayler ZE, Premke K, Gessler A, Gessner MO, Griebler C, Hilt S, Klemedtsson L, Kuzyakov Y, Reichstein M, Siemens J, Totsche K-U, Tranvik L, Wagner A, Weitere M, Grossart H-P. 2019. Integrating aquatic and terrestrial perspectives to improve insights into organic matter cycling at the landscape scale. Frontiers in Earth Science 7:127.

Lapierre JF, del Giorgio PA. 2012. Geographical and environmental drivers of regional differences in the lake pCO$_2$ versus DOC relationship across northern landscapes. Journal of Geophysical Research: Biogeosciences 117:1–10.

Lauerwald R, Regnier P, Camino-Serrano M, Guenet B, Guimberteau M, Ducharne A, Polcher J, Ciais P. 2017. ORCHILEAK (revision 3875): a new model branch to simulate carbon transfers along the terrestrial-aquatic continuum of the Amazon basin. Geoscientific Model Development 10:3821–3859.

Lukacs PM, Burnham KP, Anderson DR. 2010. Model selection bias and Freedman's paradox. Annals of the Institute of Statistical Mathematics 62:117–125.

MacIntyre S, Melack JM. 1995. Vertical and horizontal transport in lakes: linking littoral, benthic, and pelagic habitats. Journal of the North American Benthological Society 14:599–615.

MacIntyre S, Fernandes Amaral JH, Barbosa PM, Cortés A, Forsberg BR, Melack JM. 2019. Turbulence and gas transfer velocities in sheltered flooded forests of the Amazon Basin. Geophysical Research Letters 46:9628–9636.

Marotta H, Duarte CM, Sobek S, Enrich-Prast A. 2009. Large CO$_2$ disequilibria in tropical lakes. Global Biogeochemical Cycles 23:GB4022.

McDonald CP, Stets EG, Striegl RG, Butman D. 2013. Inorganic carbon loading as a primary driver of dissolved carbon dioxide concentrations in the lakes and reservoirs of the contiguous United States. Global Biogeochemical Cycles 27:285–295.

Melack JM, Engle DL. 2009. An organic carbon budget for an Amazon floodplain lake. Verhandlungen Internationale Vereinigen Limnologie 30:1179–1182.

Melo ML, Bertilsson S, Amaral JHF, Barbosa PM, Forsberg BR, Sarmento H. 2019. Flood pulse regulation of bacterioplankton community composition in an Amazonian floodplain lake. Freshwater Biology 64:108–120.

Mortillaro JM, Passarelli C, Abril G, Hubas C, Alberic P, Artigas LF, Benedetti MF, Thiney N, Moreira-Turcq P, Perez MAP, Vidal LO, Meziane T. 2016. The fate of C4 and C3 macrophyte carbon in central Amazon floodplain waters: Insights from a batch experiment. Limnologica 59:90–98.

Mortimer CH. 1952. Water movements in lakes during summer stratification – Evidence from the distribution of temperature in Windermere. Philosophical Transactions of the Royal Society of London B 236:355–404.

Piedade MTF, Junk WJ, Long SP. 1991. The productivity of the C4 grass *Echinochloa Polystachya* on the Amazon floodplain. Ecology 72:1456–1463.

Piedade MTF, Junk W, D'Ângelo SA, Wittmann F, Schöngart J, Barbosa KM do N, Lopes A. 2010. Aquatic herbaceous plants of the Amazon floodplains: state of the art and research needed. Acta Limnologica Brasiliensia 22:165–178.

Pinel S, Bonnet M-P, Da Silva JS, Sampaio TC, Garnier J, Catry T, Calmant S, Fragoso CR Jr, Moreira D, Marques DM, Seyler F. 2020. Flooding dynamics within an Amazonian floodplain: Water circulation patterns and inundation duration. Water Resources Research 56:e2019WR026081.

Premke K, Attermeyer K, Augustin J, Cabezas A, Casper P, Deumlich D, Gelbrecht J, Gerke HH, Gessler A, Grossart H-P, Hilt S, Hupfer M, Kalettka T, Kayler Z, Lischeid G, Sommer M, Zak D. 2016. The importance of landscape diversity for carbon fluxes at the landscape level: small-scale heterogeneity matters. Wires Water 3:601–617.

Quay PD, Wilbur D, Richey JE, Hedges JI, Devol AH, Victoria R. 1992. Carbon cycling in the Amazon River: Implications from the ^{13}C compositions of particles and solutes. Limnology and Oceanography 37:857–871.

R Core Team. 2020. R: A language and environment for statistical computing. R Foundation for Statistical Computing, Vienna, Austria. URL https://www.R-project.org/.

Richey JE, Devol AH, Wofsy SC, Victoria R, Riberio MNG. 1988. Biogenic gases and the oxidation and reduction of carbon in Amazon River and floodplain waters: Amazon dissolved gases. Limnology and Oceanography 33:551–561.

Richey JE, Melack JM, Aufdenkampe AK, Ballester VM, Hess LL. 2002. Outgassing from Amazonian rivers and wetlands as a large tropical source of atmospheric CO$_2$. Nature 416:617–620.

Rudorff CM, Melack JM, MacIntyre S, Barbosa CCF, Novo EMLM. 2011. Seasonal and spatial variability of CO$_2$ emission from a large floodplain lake in the lower Amazon. Journal of Geophysical Research 116:G04007.

Silva MP, Sander de Carvalho LA, Novo E, Jorge DSF, Barbosa CCF. 2020. Use of optical absorption indices to assess seasonal variability of dissolved organic matter in Amazon floodplain lakes. Biogeosciences 17:5355–5364.

Sippel S, Hamilton S, Melack J. 1992. Inundation area and morphometry of lakes on the Amazon River floodplain, Brazil. Archiv Für Hydrobiologie 123:385–400.

Smith LK, Melack JM, Hammond DE. 2003. Carbon, nitrogen and phosphorus content and ^{210}Pb-derived burial rates in sediments of an Amazon floodplain lake. Amazoniana 17:413–436.

Smith-Morrill, L. 1987. The exchange of carbon, nitrogen, and phosphorus between the sediments and water-column of an Amazon floodplain lake. Ph.D. Thesis. University of Maryland. 209 p.

Sobek S, Tranvik LJ, Cole JJ. 2005. Temperature independence of carbon dioxide supersaturation in global lakes. Global Biogeochemical Cycles 19:1–10.

Sorribas MV, Paiva RCD, Melack J, Jones C, Carvalho L, Bravo JM, Beighley E, Forsberg B, Costa MH. 2016. Projections of climate change effects on discharge and inundation in the Amazon River basin. Climatic Change 136:555–570.

Tranvik LJ, Downing JA, Cotner JB, Loiselle SA, Striegl RG, Ballatore TJ, Dillon P, Finlay K, Fortino K, Knoll LB, Kortelainen PL, Kutser T, Soren Larsen, Laurion I, Leech DM, McCallister SL, McKnight DM, Melack JM, Overholt E, Porter JA, Prairie Y, Renwick WH, Roland F, Sherman BS, Schindler DW, Sobek S, Tremblay A, Vanni MJ, Verschoor AM, von Wachenfeldt E, Weyhenmeyer GA. 2009. Lakes and reservoirs as regulators of carbon cycling and climate. Limnology and Oceanography 54:2298–2314.

Waichman AV. 1996. Autotrophic carbon sources for heterotrophic bacterioplankton in a floodplain lake of central Amazon. Hydrobiologia 341:27–36.

Ward ND, Keil RG, Medeiros PM, Brito DC, Cunha AC, Dittmar T, Yager PL, Krusche AV, Richey JE. 2013. Degradation of terrestrially derived macromolecules in the Amazon River. Nature Geoscience 6:530–533.

Weishaar JL, Aiken GR, Bergamaschi BA, Fram MS, Fujii R, Mopper K. 2003. Evaluation of specific ultraviolet absorbance as an indicator of the chemical composition and reactivity of dissolved organic carbon. Environmental Science & Technology 37:4702–4708.

Woodward BL, Marti CL, Imberger J, Hipsey MR, Oldham CE. 2017. Wind and buoyancy driven horizontal exchange in shallow embayments of a tropical reservoir: Lake Argyle, Western Australia. Limnology and Oceanography 62:1636–1657.